Electronic Supplementary Information

Isolation of the $Au_{145}(SR)_{60}X$ compound (R = *n*-butyl, *n*-pentyl; X = Br, Cl): Novel gold nanoclusters that exhibit properties subtly distinct from the ubiquitous icosahedral $Au_{144}(SR)_{60}$ compound

Tiziano Dainese, Sabrina Antonello, Sara Bonacchi, Daniel Morales-Martinez, Alfonso Venzo, David M. Black, M. Mozammel Hoque, Robert L. Whetten, and Flavio Maran

Table of Contents

1. Chemicals
2. Synthesis of $Au_{144}(SC_4H_9)_{60}$ and $Au_{144}(SC_5H_{11})_{60}$
3. Notes Regarding Mass Spectrometry
4. Figures S1-S17
5. Table S1

1. Chemicals. $HAuCl_4 \cdot 3H_2O$ (Sigma-Aldrich, 99.9%), tetra-*n*-octylammonium bromide (Sigma-Aldrich, 98%), *n*-butanethiol (Sigma-Aldrich, 99%), *n*-pentanethiol (Sigma-Aldrich, 98%), $NaBH_4$ (Sigma-Aldrich, 99%), tetrahydrofuran (THF, Sigma-Aldrich, 99.9%), toluene (Sigma-Aldrich, 99.7%), methanol (Sigma-Aldrich, 99.8%), acetone (Sigma-Aldrich, ≥99.5%), acetonitrile (Carlo Erba RS), pentane (Sigma-Aldrich, 99.8%), methylcyclohexane (Sigma-Aldrich, 99%), isopentane (Sigma-Aldrich, ≥99%), and benzene-d_6 (Sigma-Aldrich, 99.96%, d_6) were used as received. Tetra-*n*-butylammonium hexafluorophosphate (Fluka, 99%) was recrystallized from ethanol. For electrochemistry,

dichloromethane (DCM anhydrous, Sigma-Aldrich, ≥99.8%) was stored under an argon atmosphere. Low conductivity water was milliQ Water pro analysis (Merck). Column chromatography was carried out using silica gel from Macherey-Nagel (MN-Kieselgel 60 M, 230-400 mesh).

2. Synthesis of $Au_{144}(SC_4H_9)_{60}$ and $Au_{144}(SC_5H_{11})_{60}$. The synthesis of the Au_{144} clusters was performed following a literature procedure (H. Qian, R. Jin, *Chem. Mater.*, 2011, **23**, 2209–2217), with minor modifications. A typical synthesis is described for $Au_{144}(SC4)_{60}$. 0.50 g (1.27 mmol) of $HAuCl_4 \cdot 3H_2O$ was dissolved in 50 mL of methanol, and then 0.833 g of tetra-*n*-octylammonium bromide (1.52 mmol, 1.2 equiv) was added. The resulting red suspension was stirred for 30 min at 20 °C until complete dissolution of the reagents. The stirring speed was set to 100 rpm and 0.816 ml (7.62 mmol, 6 equiv) of butanethiol, dissolved in 10 mL methanol was added dropwise over a period of ~3 min. The solution quickly became a milky-white suspension. The stirring speed was increased to 600 rpm and a freshly prepared icy-cold aqueous solution (10 mL) of $NaBH_4$ (0.48 g, 12.7 mmol, 10 equiv) was quickly added to the reaction mixture. The suspension immediately became black and plenty of gas evolved. The reaction was stopped after ~12 h. The black precipitate was washed 3 times with methanol and 3 times with acetonitrile to fully remove the Au_{25} clusters. The purified product $Au_{144}(SC4)_{60}$ was finally extracted with pentane. The synthesis of $Au_{144}(SC5)_{60}$ was performed in the same way.

3. Further Notes Regarding Mass Spectrometry. We repeated certain measurements using a higher resolution (~20000:1) instrument, and could resolve the spectra with isotopic distribution (Figures S2, S5-7). The comparative abundance of ions attributable to the common byproducts - clusters of $Au_n(SR)_p$ composition (n,p) = (137,56), (130,50), (104,45), (38,24), and (25,18), all of which were readily detected in these instruments - were very low, no more than ~1% of the abundance of the main component. Figure S7 provides the assignment of the principal byproduct $Au_{137}(SC4)_{56}$, detected at a level of ~1% of the $Au_{145}(SC4)Cl_{\sim 0.7}Br_{\sim 0.3}$ sample, at isotopic resolution, with a distinctive

fragmentation pattern indicated. It is finally worth stressing that in all these analyses no instrumental separation (HPLC or trap-column insertion) has to be employed to remove small-molecule contaminants or to enhance the appearance of size-purity of the electrosprayed sample solutions.

In Figures S6-7, the experimental isotope pattern(s) of (145,60,X), (144,60), and (137,56) were shifted right to ~0.4 m/z for 3+, and ~0.3 m/z for 4+ of (144,60) to eliminate the offset due to imprecision in instrument calibration. The upper bounds on (145,60,X) from the ESI-MS results on C4 and C5 samples are limited to < 1% in comparison with (144,60) clusters. Also to be noted here, to obtain the isotopic resolution the samples were aggressively diluted, beyond what is described above, resulting in a minor trade-off in signal intensities (and hence S/N ratios). Also, thanks to this minor uncertainty (~ 1 Da) in calibration at the higher masses, one cannot rule out (or in) the presence of adventitious H^+ (protonation).

4. Figures S1-S17.

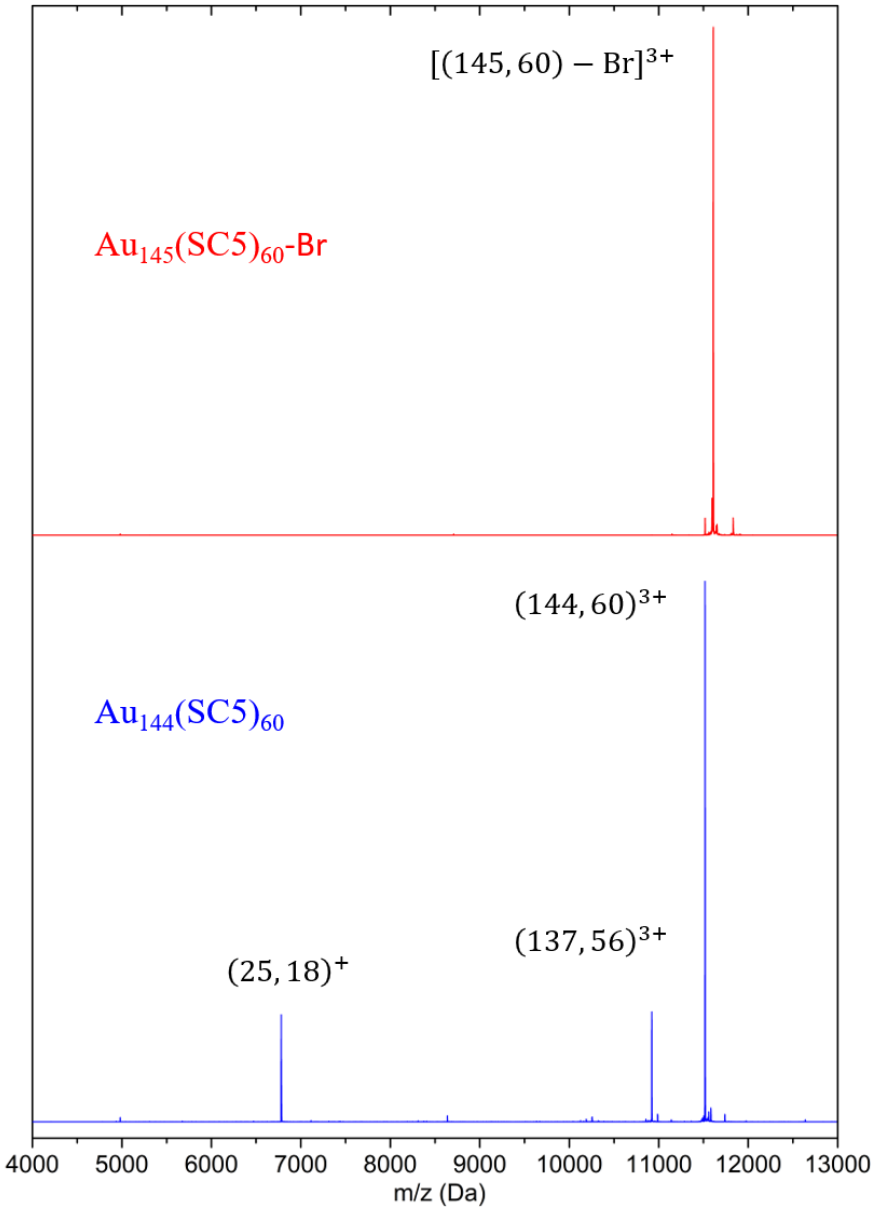

Figure S1. Positive ion mode ESI-MS detection of $[Au_{144\text{-}5}(SC5)_{60}]^{3+}$. The top frame (red trace) showing the presence of $[Au_{145}(SC5)_{60}Br]^{3+}$. The bottom frame (blue trace) showing the presence of $[Au_{144}(SC5)_{60}]^{3+}$ along with other minor products identified, i.e., $[Au_{137}(SC5)_{56}]^{3+}$ and $[Au_{25}(SC5)_{18}]^{+}$.

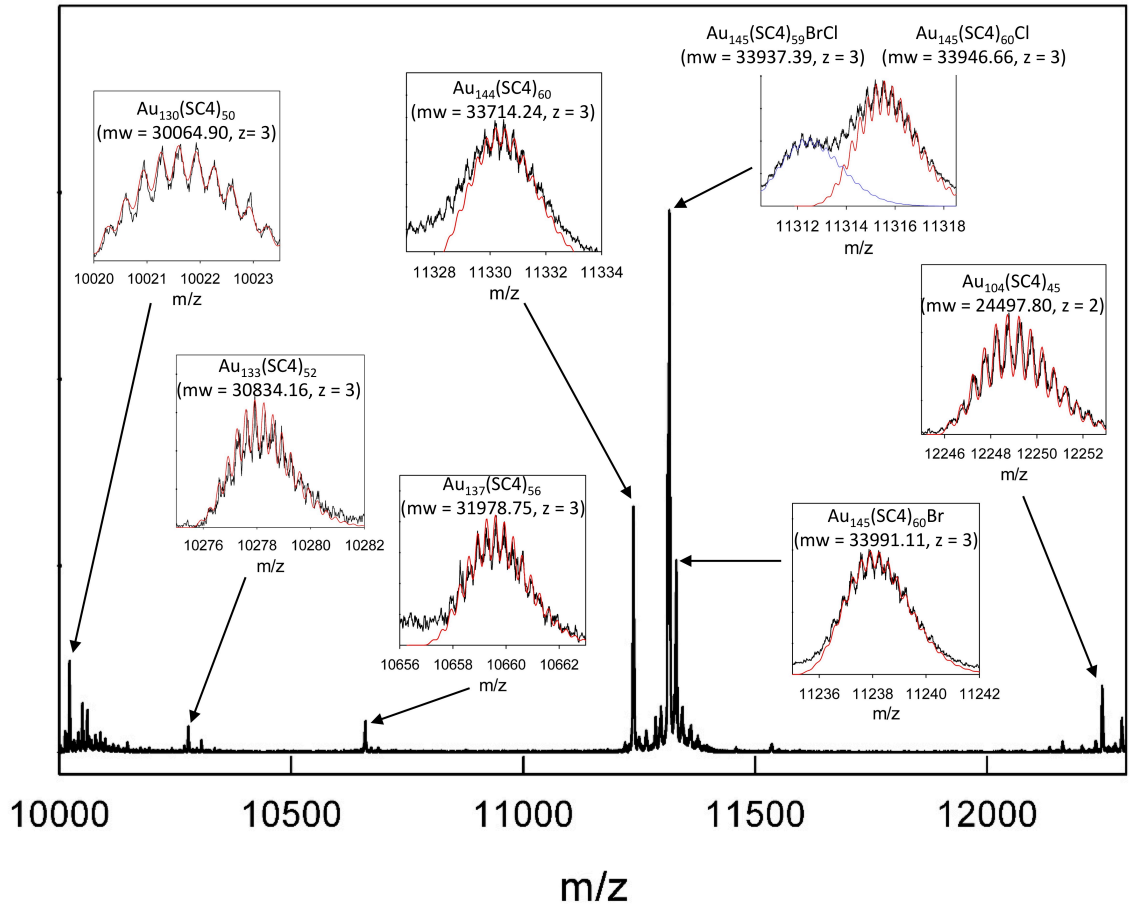

Figures S2. Details of some of the ESI-MS signals observed after 1h. Insets show experimental (black) and simulated isotopic pattern (red or blue).

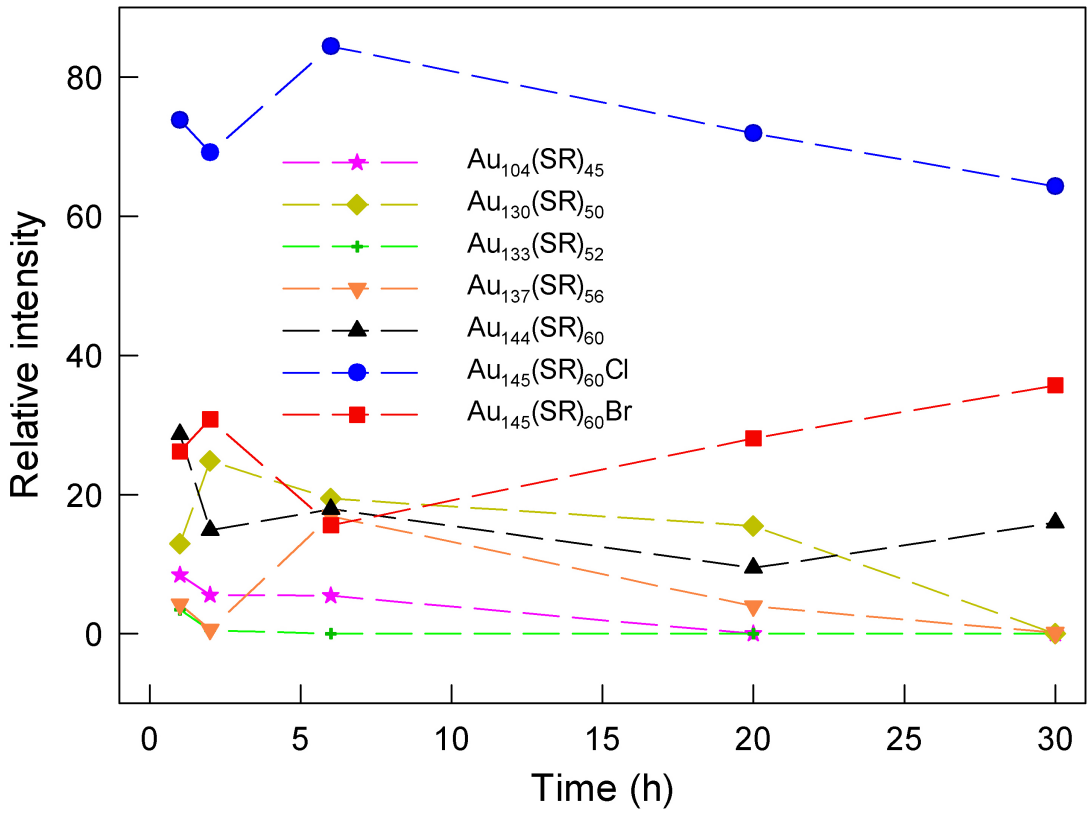

Figure S3. Time evolution of some of the ESI-MS peak intensities observed after 1, 2, 6, 20, and 30 h reaction. Intensities are normalized with respect to overall amount of $Au_{145}(SC4)_{60}X$.

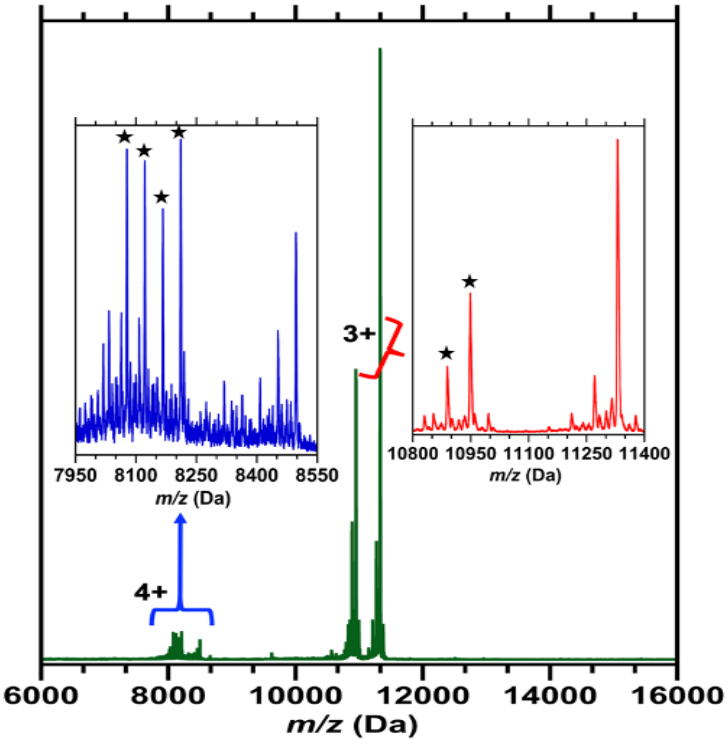

Figure S4. In-source-collision-induced-dissociation pattern for charge states 3+ and 4+ (green), ranging *m/z* 6000-16000. The inset shows the fine structure of charge state 3+ (red) and 4+ (blue); the asterisk indicates the loss of $(AuSR)_4$ [mass of ligand SC4, $S(CH_2)_3CH_3$ = 89, and Au = 197] from the surface of the gold cluster $Au_{145}(SC4)_{60}$ due to a harsh environment of the MS source.

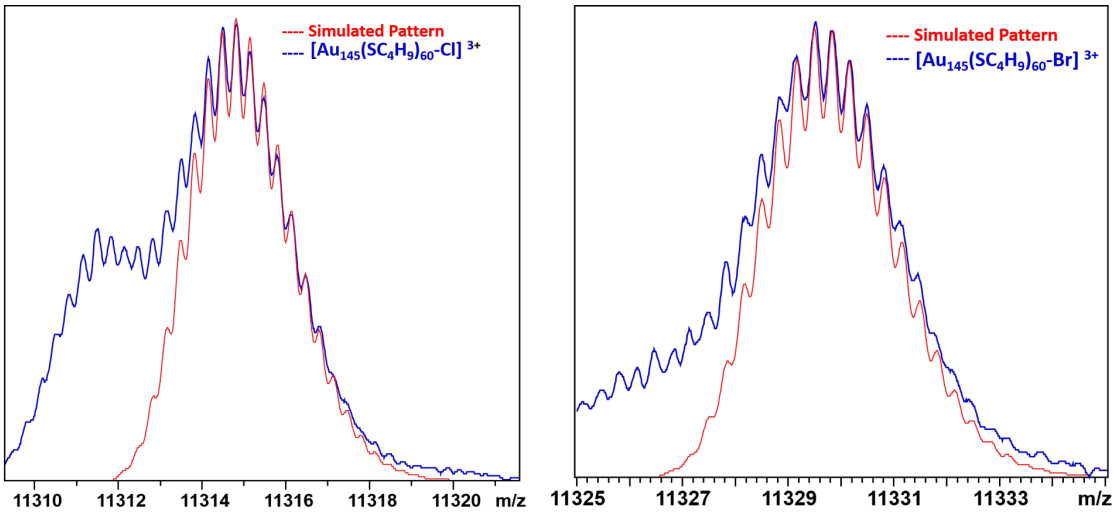

Figure S5. Isotopic pattern of $Au_{145}(SC4)_{60}X$, here X is Cl and Br. The red trace shows the pattern calculated from the formula $[Au_{145}(SC4)_{60}X]^{3+}$, whereas the blue traces show the experimental patterns of $[Au_{145}(SC4)_{60}X]^{3+}$.

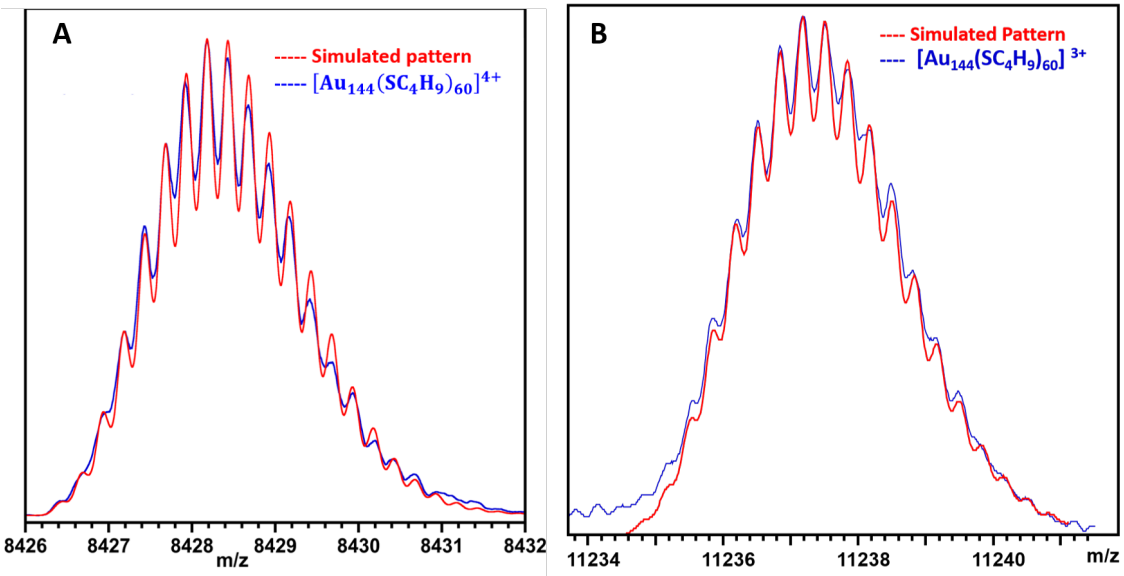

Figure S6. Isotopic resolution of the peaks assigned to $Au_{144}(SC4)_{60}^{z+}$ for z = 4+ (A) and 3+ (B). The red traces show the pattern calculated for $[Au_{144}(SC4)_{60}]^{4+}$ and $[Au_{144}(SC4)_{60}]^{3+}$. The blue traces show the experimental pattern for both charge states.

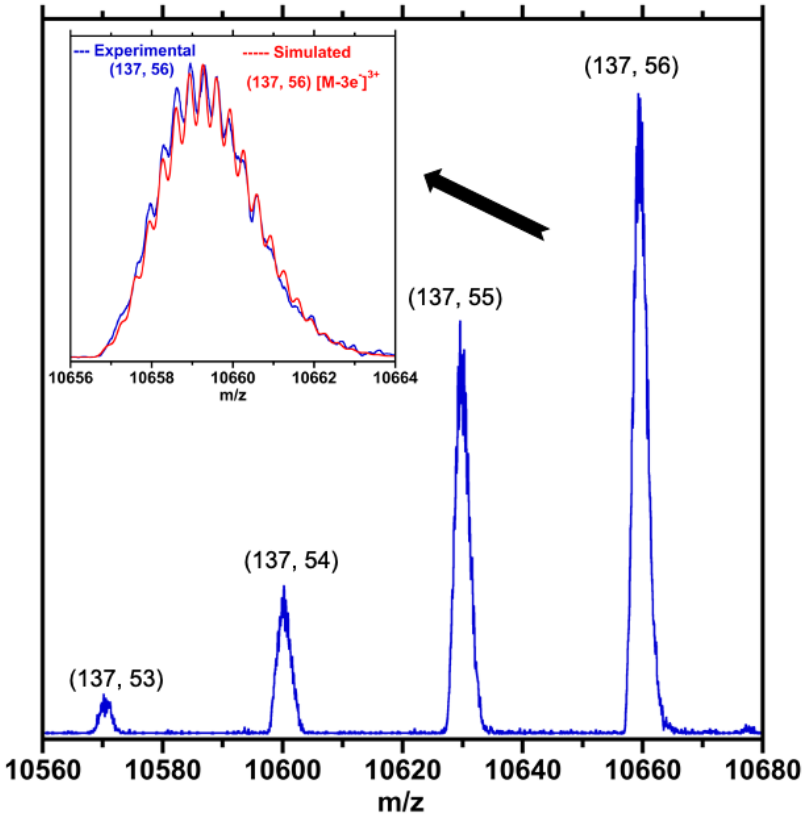

Figure S7. The presence of $Au_{137}(SC4)_X$, wherein x = 53 - 56, as a minor byproduct in the sample $Au_{145}(SC4)Cl_{\sim 0.7}Br_{\sim 0.3}$. The inset shows the isotopic pattern (in red) calculated for the composition of $[Au_{137}(SC4)_{56}]^{3+}$.

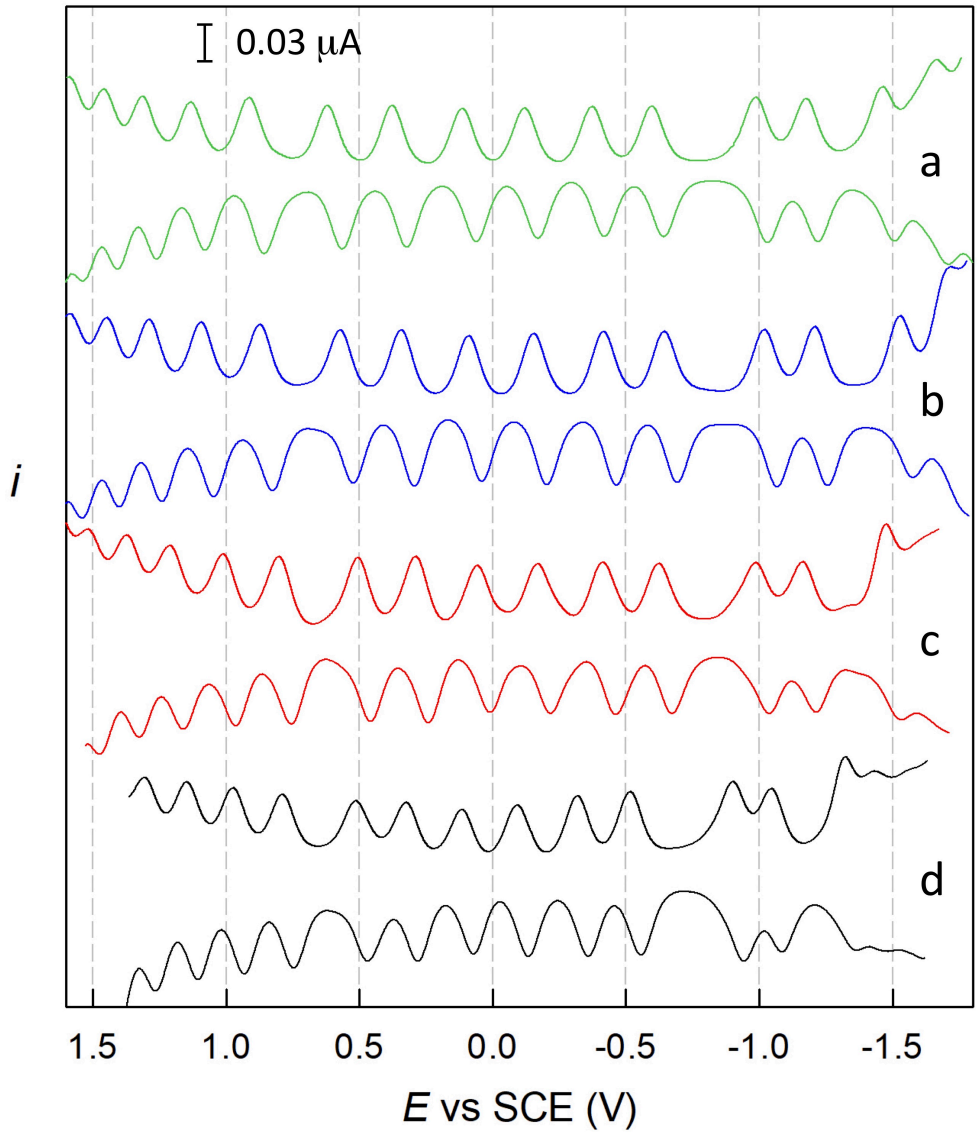

Figure S8. DPV curves for $Au_{145}(SC4)_{60}Br$ (a), $Au_{144}(SC4)_{60}$ (b), $Au_{144}(SC3)_{60}$ (c), and $Au_{144}(SC2)_{60}$ (d) in DCM/0.1 M TBAH at 20 °C on a microdisk glassy-carbon electrode.

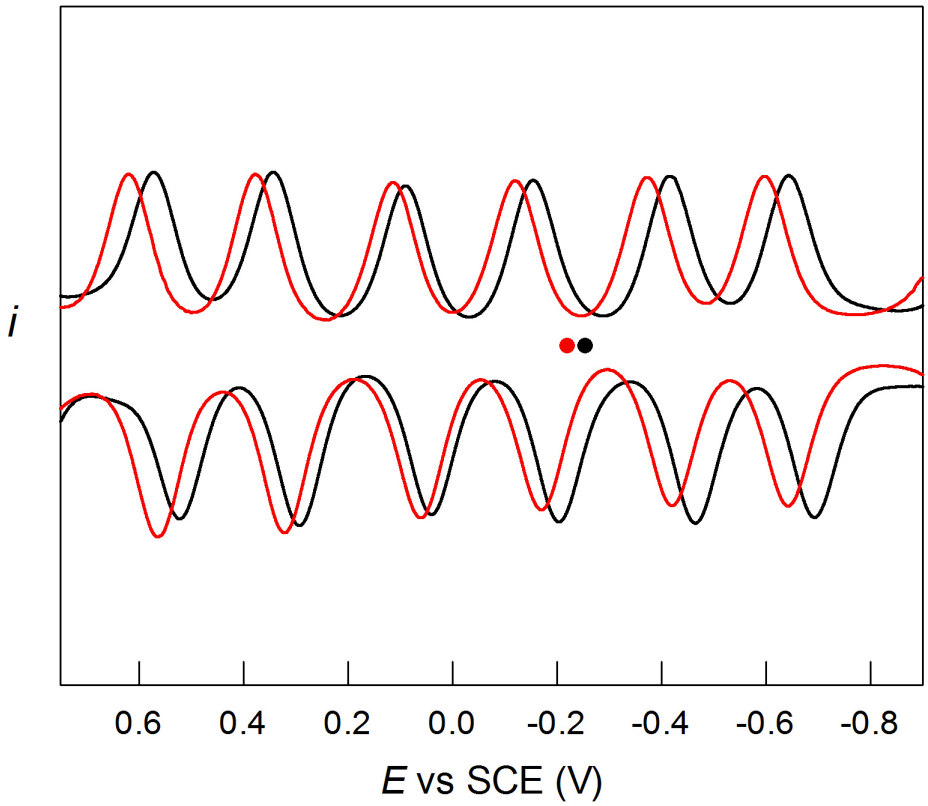

Figure S9. DPV curves for 0.16 mM $Au_{144}(SC4)_{60}$ (black curve) and 0.15 mM $Au_{145}(SC4)_{60}Br$ (red curve) in DCM/0.1 M TBAH. The potential range is limited to the six central peaks. Microdisk glassy-carbon electrode, 20 °C.

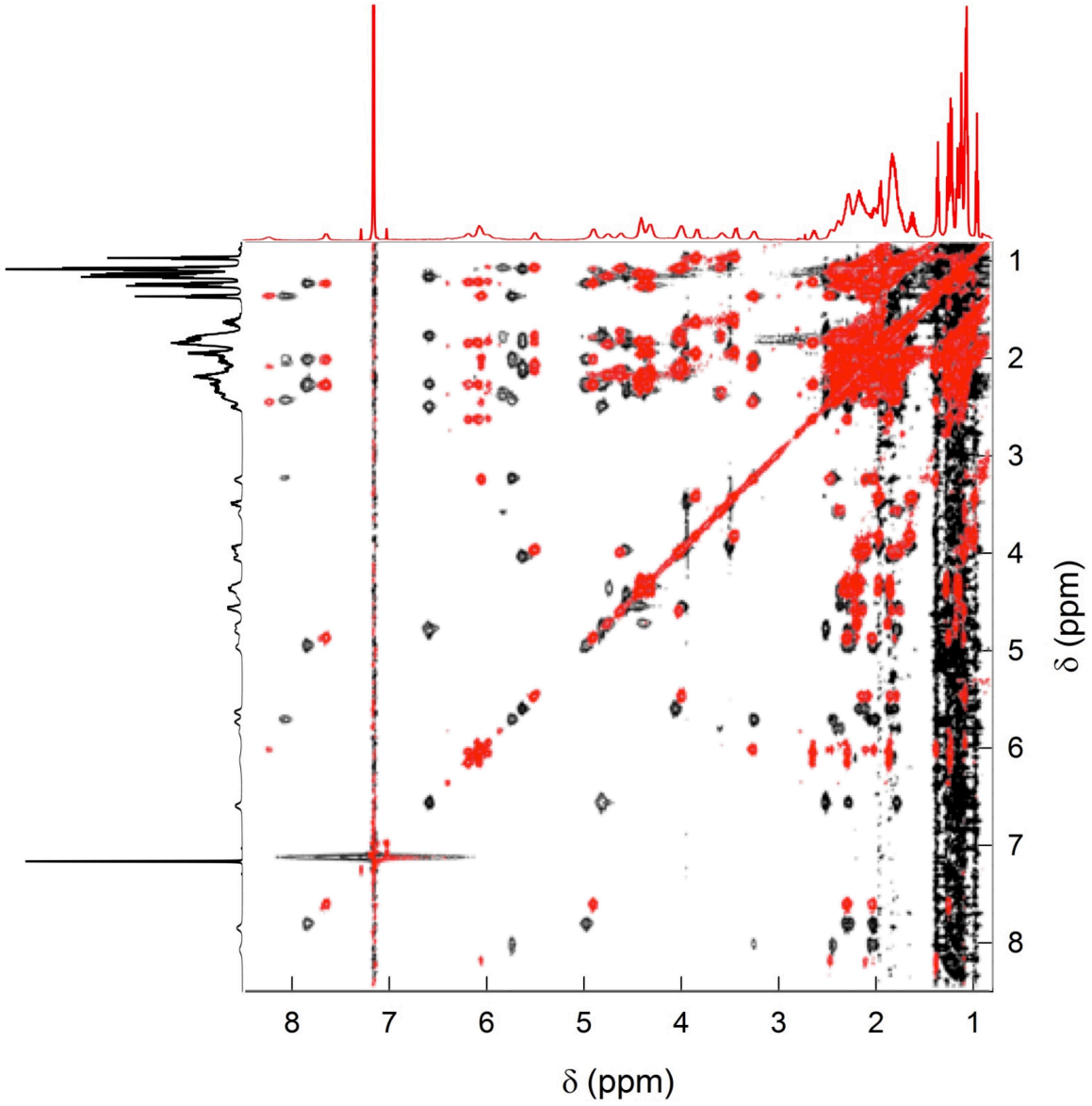

Figure S10. TOCSY spectra of 0.1 mM $Au_{145}(SC4)_{60}Br$ (red) and 0.8 mM $Au_{144}(SC4)_{60}$ (black) in C_6D_6, 45° C.

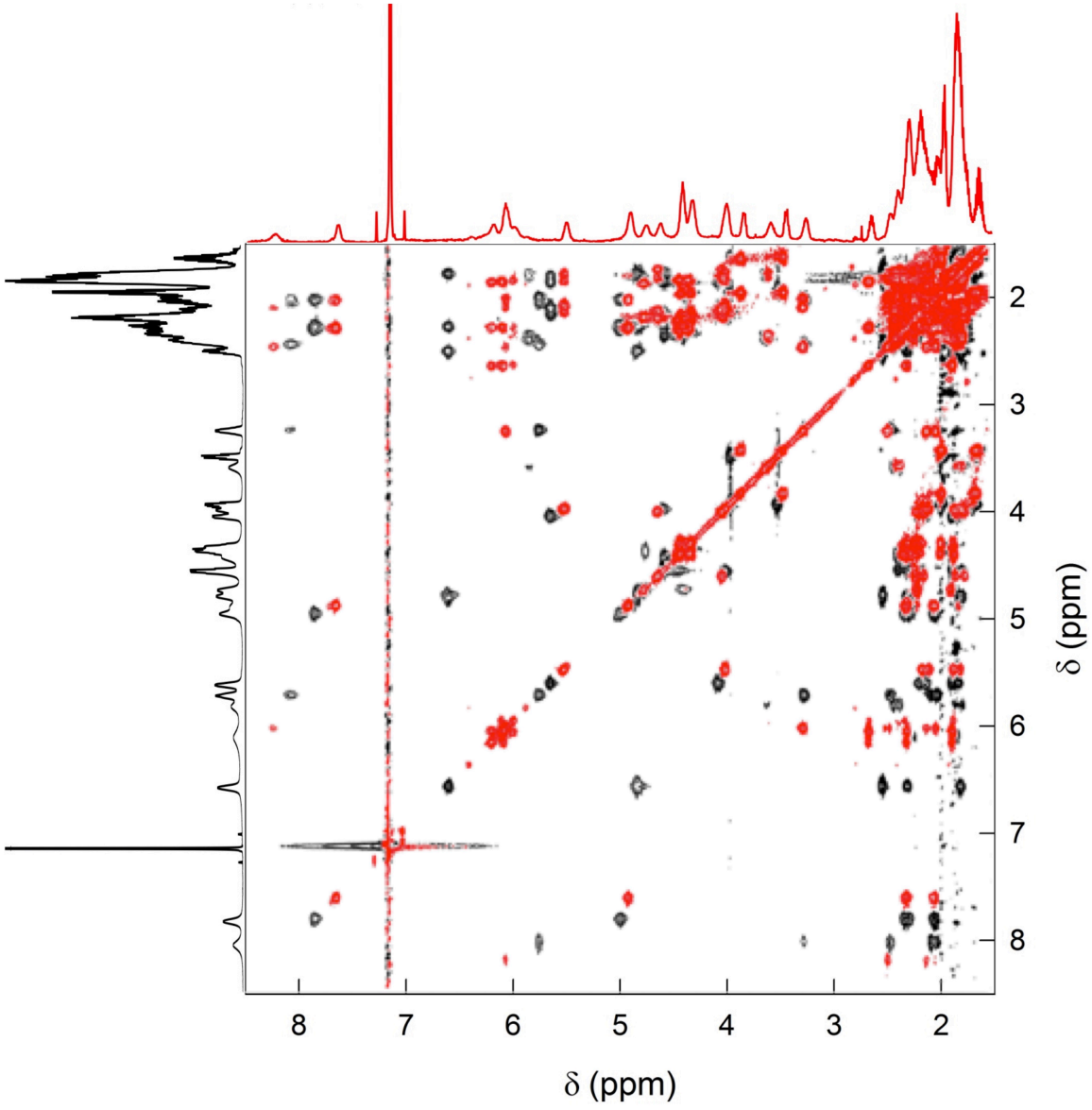

Figure S11. TOCSY spectra of 0.1 mM $Au_{145}(SC4)_{60}Br$ (red) and 0.8 mM $Au_{144}(SC4)_{60}$ (black) in C_6D_6, 45° C. The range is limited to the methylene region.

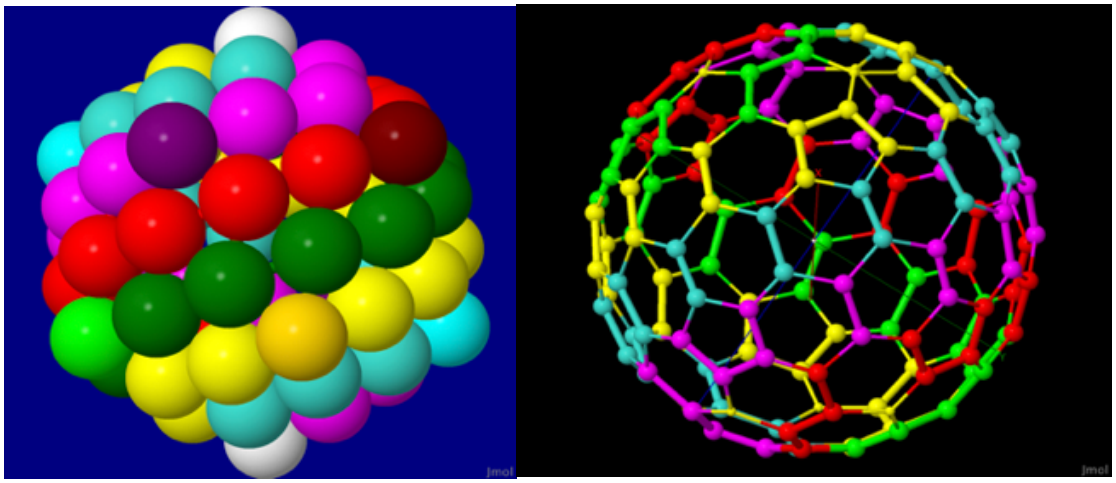

Figure S12. Schematic illustration demonstrating how, in the (144,60) and (145,60,X) systems, the icosahedral symmetry of the 60 S-atom sites (60-fold equivalence) can be compatible with the 12 distinct R-group sites, or configurations, as required by the ^{1}H-NMR spectra. Each R-group is represented here as a light-colored sphere (at left) or equivalently by a hexagon (at right); each surface void-site (on the 6 five-fold symmetry axes) is indicated by a dark sphere (left) or pentagon (right). As depicted here, the 60 R-groups are arrayed in five color-coded spirals (penta-helix) about a common five-fold axis, as mentioned just above, wherein each spiral comprises 12 distinct (*non*equivalent) R-group configurations. The X-atom (halide) site is then logically positioned at the top (or bottom) where the five spirals converge. [Source: Inspired by the Nobel Symposium Lecture, "Viruslike Clusters of Atoms", by T. P. Martin, 2001]. The coordinates at left are taken from the DFT-optimized structure of the *I*-Au*72* shell (or 'cage') structure. The coordinates for its 'dual' (at right) were taken from a database of fullerene structures, namely the chiral-icosahedral fullerene model for *I*-C_{140}. Both models have chiral-icosahedral (I-group) symmetry as established for the crystallography (and DFT predictions) of the $Au_{144}(SR)_{60}$ (z = 2+) systems.

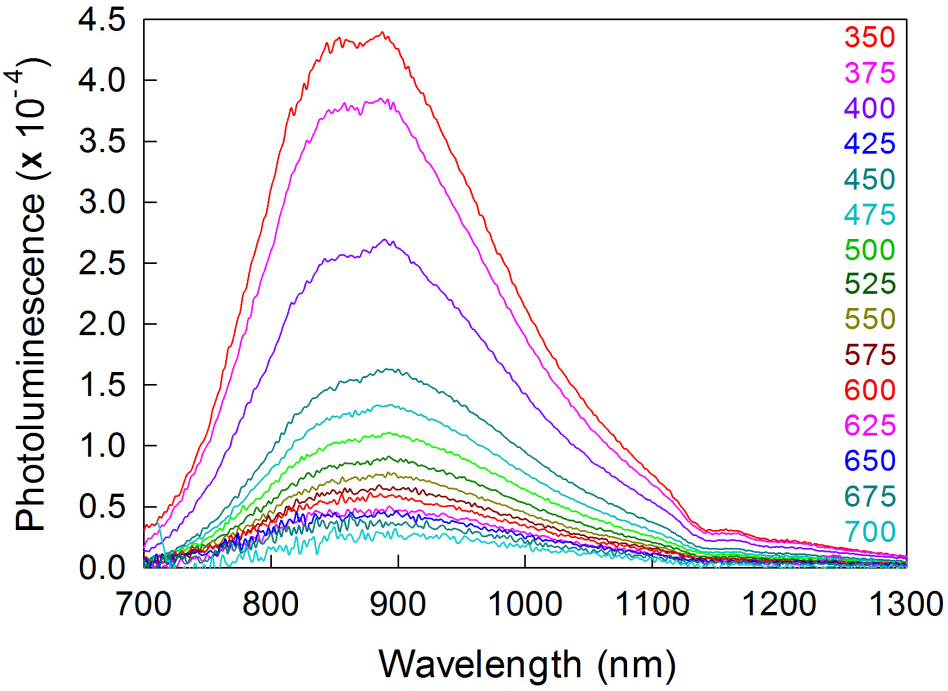

Figure S13. Excitation-emission map of $Au_{145}(SC4)_{60}X$. Absorbance 0.5 at 400 nm, toluene, room temperature. Excitation wavelengths (in nm) are indicated in the legend.

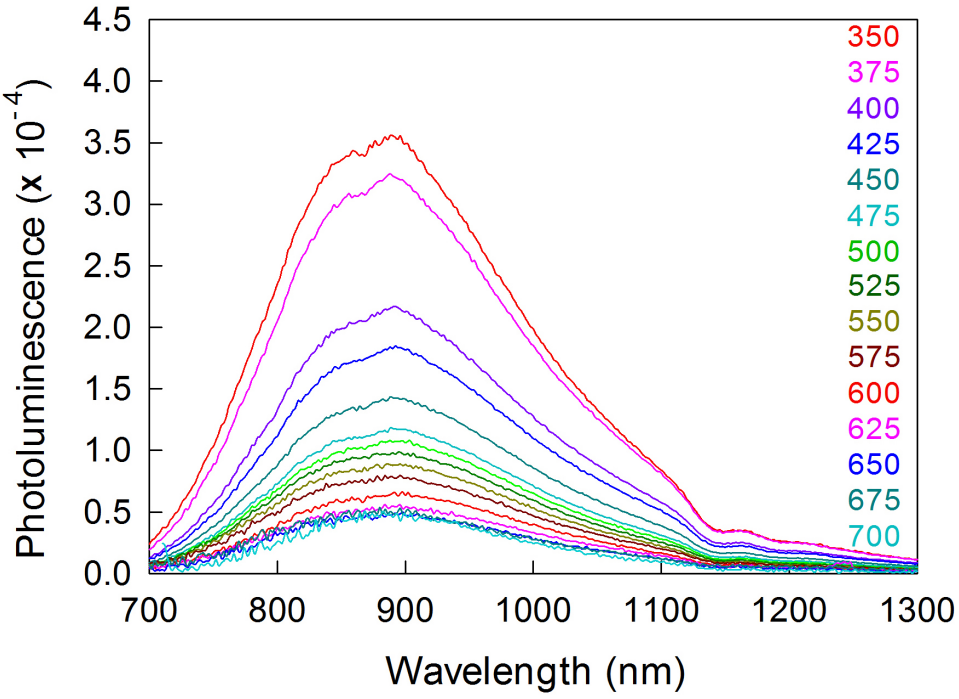

Figure S14. Excitation-emission map of $Au_{25}(SC4)_{18}$. Absorbance 0.5 at 400 nm, toluene, room temperature. Excitation wavelengths (in nm) are indicated in the legend.

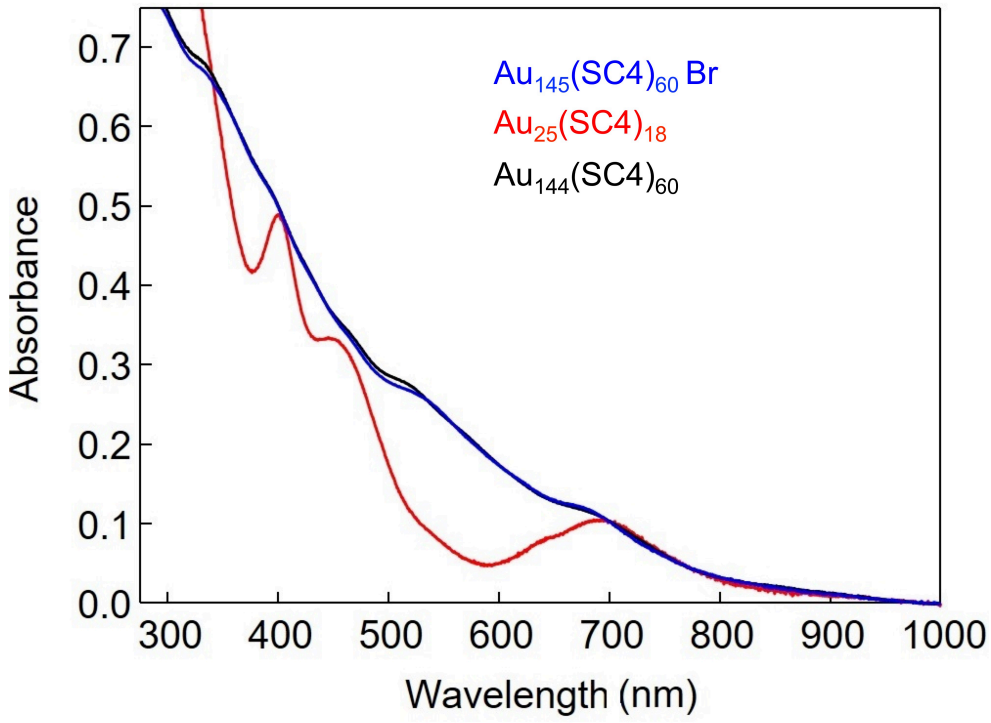

Figure S15. Absorbance (0.5 at 400 nm) of $Au_{145}(SC4)_{60}Br$ (blue), $Au_{25}(SC4)_{18}$ (red), and $Au_{144}(SC4)_{60}$ (black) in toluene at room temperature.

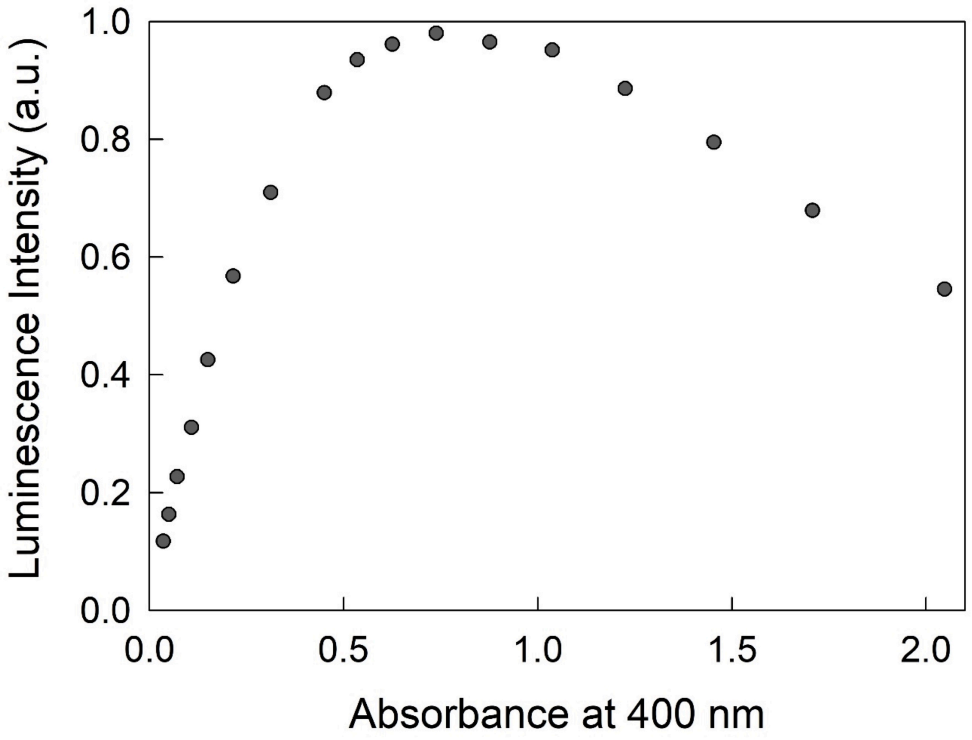

Figure S16. Luminescence intensity at 900 nm of $Au_{25}(SC4)_{18}$ in toluene obtained upon excitation at 400 nm (excitation and emission slit of 5 and 30 nm, respectively). The concentrations of the cluster (left to right) are: 0.65, 0.9, 1.3, 2.0, 2.7, 3.9, 5.7, 8.2, 9.7, 11, 13, 16, 19, 22, 26, 31, and 37 μM.

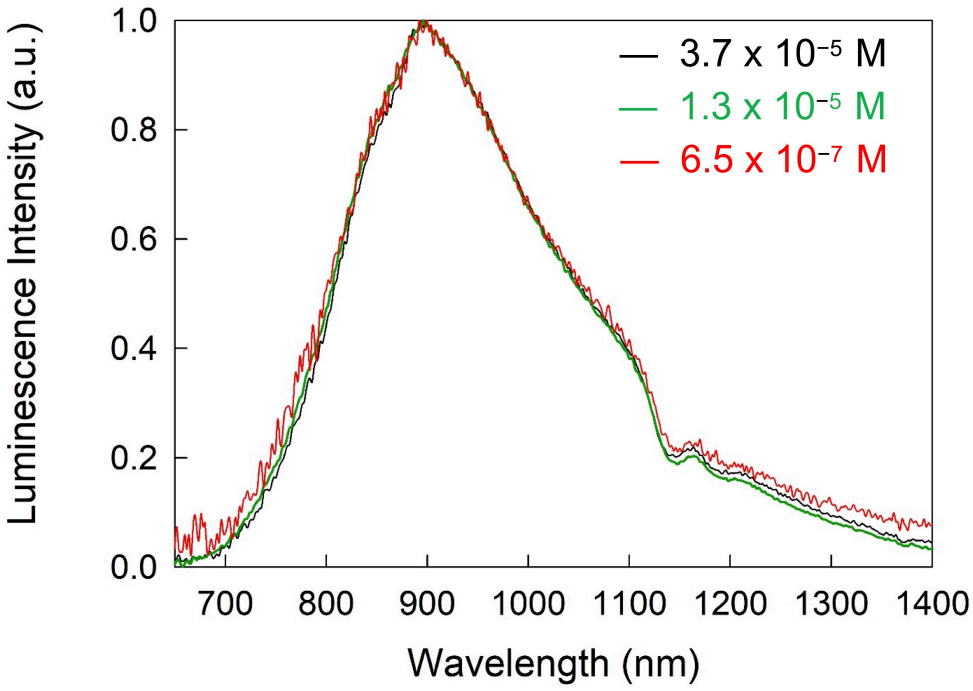

Figure S17. Luminescence of 3.7 x 10^{-5} (black), 1.3 x 10^{-5} (green), and 6.5 x 10^{-7} M (red) $Au_{25}(SC4)_{18}$ in toluene obtained upon excitation at 400 nm (excitation and emission slit of 5 and 30 nm, respectively). The spectra are normalized with respect to the luminescence maximum.

5. Table S1. ^{1}H and ^{13}C NMR data for $Au_{145}(SC4)_{60}Br$ (red) and $Au_{144}(SC4)_{60}$ (black) in C_6D_6 at 45 °C. ^{13}C NMR values are in italics, whereas the δ differences between coupled proton signals (Δδ) are in bold type. The letters mark the twelve distinct ligand types.

Type	α-CH_2	Δδ	^{13}C	β-CH_2	Δδ	^{13}C	γ-CH_2	Δδ	^{13}C	δ-CH_3	^{13}C
A	8.24 8.080	**2.20** **2.234**	*37.05* *50.7*	3.25 3.24	**0.80** **0.80**	*43.3* *43.95*	2.08 2.041	**0.08** **0.053**	*22.78* *23.12*	0.952 1.355	*12.87* *14.29*
	6.04 5.736			2.45 2.44			2.00 1.988				
B	5.49 7.841	**1.50** **2.876**	*36.93* *42.1*	2.12 2.293	**0.09** **0.041**	*39.7* *44.33*	1.83 2.026	**0.07** **0.025**	*23.0* *24.6*	1.051 1.220	*13.23* *14.94*
	3.99 4.965			2.03 2.252			1.76 2.001				
C	5.49 6.595	**0.89** **1.635**	*37.1* *38.9*	2.13 2.492	**0.07** **0.209**	*36.9* *53.08*	1.85 1.763	**0.07** **0.00**	*21.6* *26.0*	1.055 1.154	*13.25* *14.61*
	4.60 4.823			2.06 2.283			1.78 1.763				
D	5.51 6.07	**1.51** **1.172**	*37.0* *42.1*	2.13 2.274	**0.06** **0.066**	*38.06* *47.29*	1.84 1.217	**0.07** **0.00**	*24.9* *24.16*	1.056 1.080	*13.23* *14.64*
	4.00 4.898			2.07 2.208			1.77 1.217				
E	3.86 5.835	**0.41** **2.256**	*51.61* *44.6*	1.94 2.392	**0.04** **0.064**	*38.57* *49.09*	1.62 1.805	**0.02** **0.066**	*21.3* *24.40*	1.058 1.058	*12.87* *14.66*
	3.45 3.579			1.90 2.328			1.60 1.739				
F	4.60 5.733	**0.57** **2.503**	*36.8* *38.8*	2.11 2.430	**0.01** **0.08**	*40.0* *48.93*	1.80 2.18	**0.08** **0.204**	*24.8* *24.27*	1.067 1.352	*13.25* *14.96*
	4.03 3.23			2.10 2.35			1.72 1.976				
G	4.74 5.619	**0.40** **1.559**	*40.2* *54.7*	2.19 2.145	**0.04** **0.205**	*38.8* *42.56*	1.87 1.842	**0.07** **0.063**	*21.8* *23.01*	1.144 1.070	*13.1* *14.55*
	4.34 4.06			2.15 2.077			1.80 1.779				
H	6.40 4.737	**0.12** **0.367**	*59.3* *39.7*	2.26 2.186	**0.23** **0.043**	*42.2* *41.29*	2.00 1.876	**0.06** **0.047**	*21.5* *24.44*	1.214 1.050	*13.3* *14.81*
	5.84 4.376			2.23 2.143			1.86 1.829				
I	6.08 4.573	**0.10** **0.598**	*40.1* *39.8*	2.62 2.206	**0.34** **0.119**	*52.4* *40.65*	1.85 1.829	**0.02** **0.091**	*25.0* *24.37*	1.214 1.083	*13.28* *14.81*
	5.98 3.975			2.28 2.141			1.83 1.738				
J	7.68 4.531	**2.77** **0.093**	*40.81* *54.8*	2.29 2.25	**0.04** **0.299**	*40.71* *43.0*	2.02 1.831	**0.03** **0.00**	*21.53* *23.34*	1.223 1.131	*13.33* *14.28*
	4.91 4.438			2.25 2.195			1.99 1.831				
K	6.20 3.94	**0.18** **0.461**	*40.0* *37.6*	2.64 1.951	**0.03** **0.03**	*52.6* *40.14*	1.84 1.63	**0.02** **0.02**	*25.18* *22.41*	1.244 1.080	*13.41* *14.77*
	6.02 3.479			2.61 1.921			1.82 1.61				
L	8.25 4.727	**2.29** **0.383**	*37.05* *43.5*	3.24 2.196	**0.80** **0.038**	*43.4* *40.47*	2.09 1.86	**0.10** **0.018**	*23.0* *23.3*	1.365 1.148	*13.56* *14.61*
	5.96 4.344			2.44 2.158			1.99 1.842				